

# Electronic-vibrational resonance does not alter steady-state transport in natural light-harvesting systems

Leonardo F. Calderón,<sup>\*,†,‡</sup> Chern Chuang,<sup>\*,†</sup> and Paul Brumer<sup>\*,†</sup>

<sup>†</sup> *Chemical Physics Theory Group, Department of Chemistry, and Center for Quantum Information and Quantum Control, University of Toronto, Toronto, Ontario M5S 3H6, Canada*

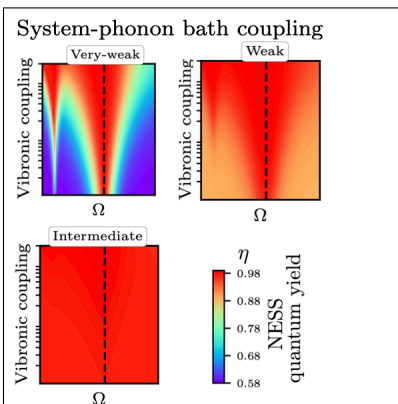
<sup>‡</sup> *Grupo de Física Computacional en Materia Condensada, Escuela de Física, Facultad de Ciencias, Universidad Industrial de Santander, Cra 27 calle 9, Bucaramanga, Colombia.*

E-mail: leonardo.calderon@utoronto.ca; chern.chuang@utoronto.ca; paul.brumer@utoronto.ca

## Abstract

Oscillations in time-dependent 2D electronic spectra appear as evidence of quantum coherence in light-harvesting systems related to electronic-vibrational resonant interactions. Nature, however, takes place in a non-equilibrium steady-state, so the relevance of these arguments to the natural process is unclear. Here we examine the role of intramolecular vibrations in the non-equilibrium steady-state of photosynthetic dimers in the natural scenario of incoherent light excitation. It is found that vibrations resonant with the energy difference between exciton states do not increase the quantum yield nor the imaginary part of the intersite coherence that is relevant for transport compared with non-resonant vibrations in the natural non-equilibrium steady state. That is, the vibration-electronic resonance interaction does not alter energy transport under natural incoherent-light excitation conditions.

## Graphical TOC Entry



Ultrafast spectroscopy has provided crucial information about the specific vibronic structure of biological light-harvesting systems and their interaction with the surrounding environment.<sup>1-6</sup> The role of intramolecular vibrations in energy transfer has been examined in coherent pulsed laser excitation studies, where it has been argued that the electronic-vibrational resonant interaction can be responsible for energy transfer enhancements, the character of quantum coherence associated with nonlinear spectroscopic signals, and for non-trivial quantum behaviour of collective pigment motions.<sup>7-28</sup> However, these laboratory-designed/controlled conditions differ fundamentally from nature,<sup>29-36</sup> where the light-harvesting systems are continuously illuminated by incoherent natural radiation (sunlight), leading to a non-equilibrium steady-state (NESS).<sup>35-39</sup> The key issue addressed in this letter is the extent to which vibration-electronic resonance affects electronic energy transport in the NESS.

We consider a prototype photosynthetic dimer to evaluate the impact of the electronic-vibrational resonance and vibronic coupling under natural incoherent light excitation. Specifically, we analyze a model PEB dimer in the cryptophyte algae PE545 antenna protein.<sup>40-42</sup> Each chromophore (PEB<sub>50/61C</sub> and PEB<sub>50/61D</sub>) is modelled as a two-level system coupled to a quantized high-energy intramolecular vibrational mode and is excitonically coupled with one another. We solve for the steady-state of this vibronic dimer (system) using an open quantum system approach. We model the sunlight as a blackbody radiation bath, the protein/solvent environment as a thermal phonon bath, and consider other processes such as exciton recombination and exciton harvesting (trapping at the reaction center), acting on nanosecond and picosecond time-scales, respectively, via effective Lindbladians.<sup>37-39,43,44</sup>

In this Letter, we analyze the different non-unitary contributions from the environment on the NESS and its relation to the vibronic effects. First, the electronic-vibrational resonance pattern is analyzed by computing the quantum yield for different Huang-Rhys factors, intramolecular vibrational frequencies, as well as the system-phonon bath coupling strengths. The quantum yield is contrasted with the imaginary part of the intersite coherence, which dictates the transport between the chromophores. We then compute the dynamics assuming

a coherent excitation initial condition to look for similarities in the vibronic resonance pattern concerning steady-state results with different system-phonon bath coupling strengths. In doing so, we demonstrate that *the vibration-electronic resonance interaction does not alter the NESS energy transport under natural incoherent-light excitation conditions*.

**Model.**—Light-induced energy transport in molecular aggregates depends on the interaction between the electronic and nuclear degrees of freedom, the latter being associated with intermolecular and intramolecular vibrations.<sup>15,45</sup> As is done here, the intermolecular vibrations are usually treated as a low-frequency continuous phonon bath described by a spectral density, and the intramolecular vibrations as discrete underdamped high-frequency vibrations.<sup>8,15</sup> In what follows, we denote the coupling and resonance interaction between electronic excitations and intramolecular vibrations as vibronic coupling and vibronic resonance, respectively.

Consider a prototype photosynthetic vibronic dimer system, immersed within a protein-solvent environment and excited by incoherent sunlight. For the  $i^{\text{th}}$  chromophore (site/molecule) only the electronic ground state  $|g_i\rangle$  and the electronic first excited state  $|\varepsilon_i\rangle$  are taken into account (two-level system approximation), and a single intramolecular vibrational mode of frequency  $\Omega_i$  per chromophore is considered. The electronic creation (annihilation) operators  $\hat{\varphi}_i^+$  ( $\hat{\varphi}_i^-$ ) are defined by  $|\varepsilon_i\rangle = \hat{\varphi}_i^+|g_i\rangle$ ,  $|g_i\rangle = \hat{\varphi}_i^-|\varepsilon_i\rangle$ . The intramolecular vibrational creation (annihilation) operators  $\hat{c}_i^\dagger$  ( $\hat{c}_i$ ) then define the intramolecular vibrational excited state  $|\chi_{i,\nu}\rangle = \left(\hat{c}_i^\dagger\right)^\nu / \sqrt{\nu!}|0_i\rangle$ , where  $\nu$  is the vibrational quantum number, and  $|0_i\rangle$  stands for the vibrational ground state. The Hamiltonian of the  $i^{\text{th}}$  chromophore reads

$$\hat{H}_i = \varepsilon_i \hat{\varphi}_i^+ \hat{\varphi}_i^- + \hbar \mathcal{G}_i \hat{\varphi}_i^+ \hat{\varphi}_i^- (\hat{c}_i^\dagger + \hat{c}_i) + \hbar \Omega_i \hat{c}_i^\dagger \hat{c}_i, \quad (1)$$

where  $\mathcal{G}_i = \Omega_i \sqrt{S_i}$  is the vibronic coupling at frequency  $\Omega_i$ , and  $S_i$  is the dimensionless Huang-Rhys factor that characterizes the electron-vibration coupling.

The global system-bath Hamiltonian reads  $\hat{H} = \hat{H}_{\text{Sys}} + \hat{H}_{\text{Sys-B}} + \hat{H}_{\text{B}}$ . Consider then a

vibronic dimer, which is the system of interest from an open quantum system perspective, composed of two interacting chromophores  $A$  (acceptor) and  $D$  (donor), where the intersite interaction is assumed to be dipolar and represented by the electronic coupling  $V_{AD}$  ( $V_{AA} = V_{DD} = 0$ ). The vibronic dimer Hamiltonian is given by

$$\hat{H}_{\text{Sys}} = \sum_i^{A,D} \varepsilon_i \hat{\varphi}_i^+ \hat{\varphi}_i^- + \sum_{i \neq j}^{A,D} V_{ij} \hat{\varphi}_i^+ \hat{\varphi}_j^- + \sum_i^{A,D} \hbar \mathcal{G}_i \hat{\varphi}_i^+ \hat{\varphi}_i^- (\hat{c}_i^\dagger + \hat{c}_i) + \sum_i^{A,D} \hbar \Omega_i \hat{c}_i^\dagger \hat{c}_i. \quad (2)$$

The intramolecular vibrational degrees of freedom are treated explicitly in the vibronic dimer model,<sup>8,15</sup> while we discuss an electronic dimer model without the former in the Supporting Information. Several discrete intramolecular vibrations are reported for cryptophyte algae.<sup>40,41</sup> Here, we performed the simulations considering different frequencies and Huang-Rhys factors to get an overall picture of the impact of the intramolecular vibrations on the NESS under incoherent light illumination. The remaining intermolecular vibrations are considered as parts of a thermal phonon bath described by a spectral density (see below).

We consider a model of the two phycoerythrobilin PEB<sub>50/61C</sub> (acceptor) and PEB<sub>50/61D</sub> (donor) chromophores (PEB dimer) from the protein-antenna phycoerythrin 545 (PE545) in cryptophyte algae. There is a large energy gap between the monomer electronic excited states  $\Delta E_e = 1042 \text{ cm}^{-1}$  and a small excitonic coupling  $V_{AD} = 92 \text{ cm}^{-1}$  between the PEB dimer. Exciton states are highly localized over a specific chromophore, and the exciton energy gap is  $\Delta E_e = 1058 \text{ cm}^{-1}$ . The transition dipole moments are 12.17 D (PEB<sub>50/61C</sub>) and 11.87 D (PEB<sub>50/61D</sub>). We assume that both chromophores have the same intramolecular vibrational frequencies and vibronic couplings, i.e.,  $\Omega = \Omega_A = \Omega_D$  and  $\mathcal{G} = \mathcal{G}_A = \mathcal{G}_D$ . The first three levels of quantized intramolecular vibrations are considered in the simulations below.

*Interaction with the environment.*—The system-bath and bath Hamiltonians read

$$\hat{H}_{\text{Sys-B}} = \sum_i^{A,D} \sum_l \hbar g_{il}^{(e)} \hat{\varphi}_i^+ \hat{\varphi}_i^- \left( \hat{b}_l^{(i)} + \hat{b}_l^{(i)\dagger} \right) + \sum_i^{A,D} \sum_m \hbar g_{im}^{(v)} (\hat{c}_i^\dagger + \hat{c}_i) \left( \hat{b}_m^{(i)} + \hat{b}_m^{(i)\dagger} \right) - \sum_i \hat{\boldsymbol{\mu}}_i \cdot \hat{\mathbf{E}}(t), \quad (3)$$

$$\hat{H}_B = \sum_i \sum_l^{A,D} \hbar \omega_l^{(i)} \hat{b}_l^{(i)\dagger} \hat{b}_l^{(i)} + \sum_i \sum_m^{A,D} \hbar \omega_m^{(i)} \hat{b}_m^{(i)\dagger} \hat{b}_m^{(i)} + \sum_{\mathbf{k},s} \hbar c k \hat{a}_{\mathbf{k},s}^\dagger \hat{a}_{\mathbf{k},s}. \quad (4)$$

Here,  $g_{il}^{(e)}$  ( $g_{im}^{(v)}$ ) represents the coupling between the electronic (intramolecular vibrational) degrees of freedom of the  $i^{\text{th}}$  chromophore and the  $l^{\text{th}}$  ( $m^{\text{th}}$ ) phonon mode, where  $\hat{b}_l^{(i)\dagger}, \hat{b}_m^{(i)\dagger}$  ( $\hat{b}_l^{(i)}, \hat{b}_m^{(i)}$ ) are the creation (annihilation) operators of the phonon modes of frequencies  $\omega_l^{(i)}, \omega_m^{(i)}$  that couple to the electronic and intramolecular vibrational degrees of freedom of the  $i^{\text{th}}$  chromophore. The electric field of the radiation<sup>46</sup> is given by  $\hat{\mathbf{E}}(t) = \hat{\mathbf{E}}^{(+)}(t) + \hat{\mathbf{E}}^{(-)}(t)$ , with  $\hat{\mathbf{E}}^{(+)}(t) = i \sum_{\mathbf{k},s} \left( \frac{\hbar \omega}{2\epsilon_0 V} \right)^{1/2} \hat{a}_{\mathbf{k},s}(\epsilon_{\mathbf{k},s}) e^{-i\omega t}$  and  $\hat{\mathbf{E}}^{(-)}(t) = \left[ \hat{\mathbf{E}}^{(+)}(t) \right]^\dagger$ , with  $\hat{a}_{\mathbf{k},s}^\dagger$  ( $\hat{a}_{\mathbf{k},s}$ ) being the creation (annihilation) operator for the  $\mathbf{k}^{\text{th}}$  radiation field mode in the  $s^{\text{th}}$  polarization state, and  $\hat{\boldsymbol{\mu}}_i$  is the dipole operator for the  $i^{\text{th}}$  chromophore.

The open quantum system dynamics of the density operator  $\hat{\rho}$  for the vibronic dimer system described in Eq. 2 is given by the master equation

$$\frac{\partial}{\partial t} \hat{\rho} = -\frac{i}{\hbar} [\hat{H}_{\text{Sys}}, \hat{\rho}] + \mathcal{L}_{\text{RB}} [\hat{\rho}] + \mathcal{L}_{\text{PB}} [\hat{\rho}] + \mathcal{L}_{\text{rec}} [\hat{\rho}] + \mathcal{L}_{\text{trap}} [\hat{\rho}]. \quad (5)$$

The first term on the right-hand side describes the unitary evolution of the dimer system. The Liouvillian operator for the incoherent radiation environment (blackbody radiation bath denoted as RB) and the protein/solvent environment (phonon baths denoted as PB) read  $(\mathcal{L}_{\text{RB,PB}} [\hat{\rho}])_{ij} = -\sum_{kl} R_{ij,kl}^{\text{RB,PB}} \rho_{kl}(t)$ , where we use the standard non-secular Redfield approach for thermal baths comprised of harmonic modes<sup>45,47</sup>

$$R_{ij,kl}^{\text{RB,PB}} = \delta_{ik} \sum_m \Gamma_{jm,ml}^{\text{RB,PB}}(\omega_{lm}) + \delta_{jl} \sum_m \Gamma_{im,mk}^{\text{RB,PB}}(\omega_{km}) - \Gamma_{ki,jl}^{\text{RB,PB}}(\omega_{lj}) - \Gamma_{lj,ik}^{\text{RB,PB}}(\omega_{ki}). \quad (6)$$

The damping matrix elements

$$\Gamma_{ij,kl}^{\text{RB,PB}}(\omega) = \sum_{u,v} \int_0^\infty dt e^{i\omega t} C_{u,v}^{\text{RB,PB}}(t) K_{u,ij}^{\text{RB,PB}} K_{v,kl}^{\text{RB,PB}}, \quad (7)$$

determine the time span for correlations. Here,  $K_{u,ij}^{\text{RB,PB}}$  denote the observables of the vibronic

dimer system that are coupled to the radiation and phonon baths modes (see Eq. 3), and

$$C_{u,v}^{\text{RB,PB}}(t) = \int_0^\infty d\omega \omega^2 J_i^{\text{RB,PB}}(\omega) \left[ \coth\left(\frac{\hbar\omega\beta}{2}\right) \cos(\omega t) - i \sin(\omega t) \right], \quad (8)$$

the correlation functions of the radiation and phonon baths. Formally, the radiation bath is described by a super-Ohmic spectral density with cubic-frequency dependence which generates long-lasting coherent dynamics provided by the lack of pure dephasing dynamics and the strong dependence of the decoherence rate on the system level spacing<sup>34</sup>

$$\omega^2 J_j^{\text{RB}}(\omega) = \frac{2\hbar\omega^3}{3(4\epsilon_0\pi^2 c^3)}. \quad (9)$$

The phonon baths introduce dissipation and decoherence into the electronic (e) and intramolecular vibrational (v) degrees of freedom of the system Hamiltonian (Eq. 2). Its effects are encoded in the Drude-Lorentz spectral density

$$\omega^2 J_j^{\text{PB}}(\omega) = \frac{2\gamma_j^{(\text{e,v})} \lambda_j^{(\text{e,v})} \omega}{\hbar(\omega^2 + \gamma_j^{(\text{e,v})2})}, \quad (10)$$

where  $\gamma^{(\text{e,v})}$  represents the cutoff frequency and  $\lambda^{(\text{e,v})}$  the reorganization energies. The same spectral densities are assumed on each chromophore, with  $\gamma_{A,D}^{(\text{e,v})} = 100 \text{ cm}^{-1}$  and different values for  $\lambda_{A,D}^{(\text{e,v})}$  below. The temperature assumed for the phonon bath it is  $T^{\text{PB}} = 300 \text{ K}$ , and  $T^{\text{RB}} = 5600 \text{ K}$  for the blackbody radiation bath. The transition dipole moments of the chromophores are considered constants in time and parallel to the incoherent light electric field.

The exciton recombination and the trapping at the reaction center processes are considered localized processes on each chromophore<sup>37–39,43,44</sup> and modelled through the effective Lindbladians

$$\mathcal{L}_{\text{rec}}[\hat{\rho}] = \tau_{\text{rec}}^{-1} \sum_i^{A,D} \left( |g_i\rangle \langle \varepsilon_i| \hat{\rho} |\varepsilon_i\rangle \langle g_i| - \frac{1}{2} [|\varepsilon_i\rangle \langle \varepsilon_i|, \hat{\rho}]_+ \right), \quad (11)$$

$$\mathcal{L}_{\text{trap}}[\hat{\rho}] = \tau_{\text{trap}}^{-1} \left( |\text{RC}\rangle \langle \varepsilon_A| \hat{\rho} | \varepsilon_A\rangle \langle \text{RC}| - \frac{1}{2} [|\varepsilon_A\rangle \langle \varepsilon_A|, \hat{\rho}]_+ \right), \quad (12)$$

where  $[\hat{\mathcal{O}}_1, \hat{\mathcal{O}}_2]_+$  represents the anticommutator between operators  $\hat{\mathcal{O}}_1$  and  $\hat{\mathcal{O}}_2$ . The recombination mechanism (Eq. 11) accounts for the electronic excitation decay to the ground state due to nonradiative processes, and is determined by the recombination time  $\tau_{\text{rec}}$ , which is assumed the same for both chromophores. The trapping process (Eq. 12) dictates the electronic excitation harvesting at the reaction center from the acceptor chromophore on a time scale determined by the trapping time  $\tau_{\text{trap}}$ . Recombination and trapping times are expected to be on the order of nanoseconds and picoseconds, respectively.<sup>41,43,48</sup>

**Energy transport.**—We assume that only the donor chromophore  $D$  interacts with the incoherent light and the acceptor chromophore  $A$  has a lower electronic excitation energy, i.e.,  $\varepsilon_D > \varepsilon_A$ . To analyze the transport between chromophores, note that the Hamiltonian of the vibronic dimer (Eq. 2) in the electronic-vibrational localized state basis (single-excitation manifold)  $\{|g_j^\beta \varepsilon_i^\alpha\rangle = |\chi_{j,\beta}^{(g)}, g_j, \chi_{i,\alpha}^{(\varepsilon)}, \varepsilon_i\rangle\}$  is given by

$$\begin{aligned} \hat{H}_{\text{Sys}} = & \sum_{i \neq j} \sum_{\alpha, \beta}^{A,D} \varepsilon_i |g_j^\beta \varepsilon_i^\alpha\rangle \langle \varepsilon_i^\alpha g_j^\beta| + \sum_{i \neq j} \sum_{\alpha, \beta}^{A,D} V_{ij} |g_j^\beta \varepsilon_i^\alpha\rangle \langle \varepsilon_j^\alpha g_i^\beta| \\ & + \sum_{i \neq j} \sum_{\alpha, \nu, \mu}^{A,D} \hbar \mathcal{G}_i \left( \delta_{\nu, \mu+1} \sqrt{\mu+1} + \delta_{\nu, \mu-1} \sqrt{\mu} \right) |g_j^\alpha \varepsilon_i^\nu\rangle \langle \varepsilon_i^\mu g_j^\alpha| + \sum_{i \neq j} \sum_{\alpha, \beta}^{A,D} \alpha \hbar \Omega_i |g_j^\beta \varepsilon_i^\alpha\rangle \langle \varepsilon_i^\alpha g_j^\beta|. \end{aligned} \quad (13)$$

The first term of the right-hand side of Eq. 13 accounts for the electronic site energies, the second stands for the excitonic coupling, the third is the vibronic coupling, and the last is the vibrational energy.

The change in the population of the state  $|g_D^\mu \varepsilon_A^\nu\rangle$  (see Eqs. 5 and 13) is equal to

$$\begin{aligned} \langle g_D^\mu \varepsilon_A^\nu | \dot{\hat{\rho}} | g_D^\mu \varepsilon_A^\nu \rangle = & 2V_{AD} \text{Im} [\rho_{DA}^{\nu, \mu; \nu, \mu}] + 2\hbar \mathcal{G}_A \left( \sqrt{\nu} \text{Im} [\rho_{AA}^{\nu-1, \mu; \nu, \mu}] + \sqrt{\nu+1} \text{Im} [\rho_{AA}^{\nu+1, \mu; \nu, \mu}] \right) \\ & - \tau_{\text{rec}}^{-1} \rho_{AA}^{\nu, \mu; \nu, \mu} - \tau_{\text{trap}}^{-1} \rho_{AA}^{\nu, \mu; \nu, \mu}. \end{aligned} \quad (14)$$

The unitary contributions to the change in the population of the acceptor state  $|g_D^\mu \varepsilon_A^\nu\rangle$  originate from the electronic interaction ( $V_{AD}$ ) with the donor state  $|g_A^\mu \varepsilon_D^\nu\rangle$  through the imaginary part of the coherence density matrix element  $\rho_{DA}^{\nu,\mu;\nu,\mu}$ , and from the vibronic interaction  $\mathcal{G}_A$  with acceptor states with adjacent vibrational numbers  $\nu - 1$  and  $\nu + 1$ . The non-unitary contributions arise from recombination and trapping. It should be noted that the phonon baths do not contribute directly to the change of the population of the state  $|g_D^\mu \varepsilon_A^\nu\rangle$  due to the pure dephasing interaction in the system-bath Hamiltonian<sup>39,49</sup> (see Eq. 3).

By tracing over all the vibrational states, the change in the population at the acceptor chromophore reads

$$\frac{dP_A}{dt} = \sum_{\nu,\mu} \langle g_D^\mu \varepsilon_A^\nu | \dot{\rho} | g_D^\mu \varepsilon_A^\nu \rangle = 2V_{AD} \text{Im} [\rho_{DA}] - (\tau_{\text{rec}}^{-1} + \tau_{\text{trap}}^{-1}) \rho_{AA}, \quad (15)$$

where  $\text{Im} [\rho_{DA}] = \sum_{\nu,\mu} \text{Im} [\rho_{DA}^{\nu,\mu;\nu,\mu}]$  and  $\rho_{AA} = \sum_{\nu,\mu} \rho_{AA}^{\nu,\mu;\nu,\mu}$ , which are the intersite coherence and acceptor population of the electronic subsystem. The second term on the right-hand side of Eq. 14 disappears since contributions from different vibrational levels on the acceptor add up to zero. From Eq. 15 it can be inferred that the flux from the donor chromophore is  $F_{DA} = 2V_{AD} \text{Im} [\rho_{DA}]$ . The above allows us to connect with the case of transport in an electronic dimer without intramolecular vibrational modes,<sup>39</sup> i.e. without the effects of vibronic resonance.

**Quantum yield: Energy transfer efficiency.**—We consider a definition for the quantum yield  $\eta$  based on currents<sup>38,44</sup> (transfer rates)

$$\eta = \frac{\mathcal{J}_{\text{trap}}}{\mathcal{J}_{\text{abs}}}, \quad (16)$$

where the  $\mathcal{J}_{\text{trap}} = \sum_i \langle \psi_i^{(e)} | \mathcal{L}_{\text{trap}} [\hat{\rho}] | \psi_i^{(e)} \rangle$  is the current of trapping at the reaction center, and  $\mathcal{J}_{\text{abs}} = \sum_i \langle \psi_i^{(e)} | \mathcal{L}_{\text{RB}}^{(\text{abs})} [\hat{\rho}] | \psi_i^{(e)} \rangle$  is the incoherent light absorption current. Note that  $\mathcal{J}_{\text{trap}} \neq \tau_{\text{trap}}^{-1}$  (see Eq. 12). The states  $|\psi_i^{(e)}\rangle$  are (single-excitation manifold) eigenstates of the vibronic dimer Hamiltonian,  $\hat{H}_{\text{Sys}} |\psi_i^{(e)}\rangle = E_i |\psi_i^{(e)}\rangle$ . While both currents  $\mathcal{J}_{\text{trap}}$  and

$\mathcal{J}_{\text{abs}}$  contribute to the determination of the quantum yield, we find that  $\mathcal{J}_{\text{abs}}$  is essentially constant. This suggests that the changes in the quantum yield are mainly dependent on the trapping current  $\mathcal{J}_{\text{trap}}$ .

In the steady-state regime, the following continuity equation must be satisfied

$$\frac{\mathcal{J}_{\text{emi}} + \mathcal{J}_{\text{rec}} + \mathcal{J}_{\text{trap}}}{\mathcal{J}_{\text{abs}}} = 1. \quad (17)$$

Here,  $\mathcal{J}_{\text{emi}} = \sum_i \langle \psi_i^{(e)} | \mathcal{L}_{\text{RB}}^{(emi)} [\hat{\rho}] | \psi_i^{(e)} \rangle$  and  $\mathcal{J}_{\text{rec}} = \sum_i \langle \psi_i^{(e)} | \mathcal{L}_{\text{rec}} [\hat{\rho}] | \psi_i^{(e)} \rangle$  denote the incoherent light emission and recombination currents, respectively. The incoherent light currents  $\mathcal{J}_{\text{abs}}$  and  $\mathcal{J}_{\text{emi}}$  are related to the blackbody radiation bath occupation number  $(e^{\hbar\omega/k_B T^{\text{RB}}} - 1)^{-1}$ ,  $\omega \geq 0$  (absorption) and  $(e^{\hbar\omega/k_B T^{\text{RB}}} - 1)^{-1} + 1$ ,  $\omega < 0$  (emission).<sup>38</sup> From Eq. 17, it can be concluded that the quantum yield  $\eta = 1$  when  $\mathcal{J}_{\text{emi}} = \mathcal{J}_{\text{rec}} = 0$ . Although, the current definitions discussed above have been described for the single-excitation eigenstate manifold, their definitions are basis-invariant,<sup>44</sup> i.e., the sum  $\sum_i \langle \psi_i^{(e)} | \dots | \psi_i^{(e)} \rangle$  represents the trace over the system of interest.

***Quantum yield under an electronic-vibrational resonance interaction.***— Given the recent interest in the potential quantum effects and energy transfer enhancements driven by the electronic-vibrational resonance interaction,<sup>19,24,25</sup> we first compute the steady-state  $\frac{\partial \rho_{\text{SS}}}{\partial t} = 0$  in Eq. 5 for different values of the intramolecular vibrational frequency  $\Omega$  close to the exciton energy gap  $\Delta E_e = 1058 \text{ cm}^{-1}$  (vibronic resonance) and Huang-Rhys factors  $S$  (vibronic coupling strengths) reported for cryptophyte algae.<sup>40,41</sup> To quantify a possible effect due to the vibronic resonance, Figure 1 shows the quantum yield (top panels) as a function of the intramolecular vibrational frequency  $\Omega$  and the Huang-Rhys factor  $S$  for selected values of the system-phonon bath coupling strength  $\lambda^{(e,v)}$ . We assume typical values for recombination  $\tau_{\text{rec}} = 1 \text{ ns}$  and trapping  $\tau_{\text{trap}} = 10 \text{ ps}$  times (See Figure S1 presented in the Supporting Information where a trapping time  $\tau_{\text{trap}} = 1 \text{ ps}$  is considered). A vertical dashed line in Figure 1 indicates the on-resonance intramolecular vibrational frequency  $\Omega = 1058 \text{ cm}^{-1}$ , and

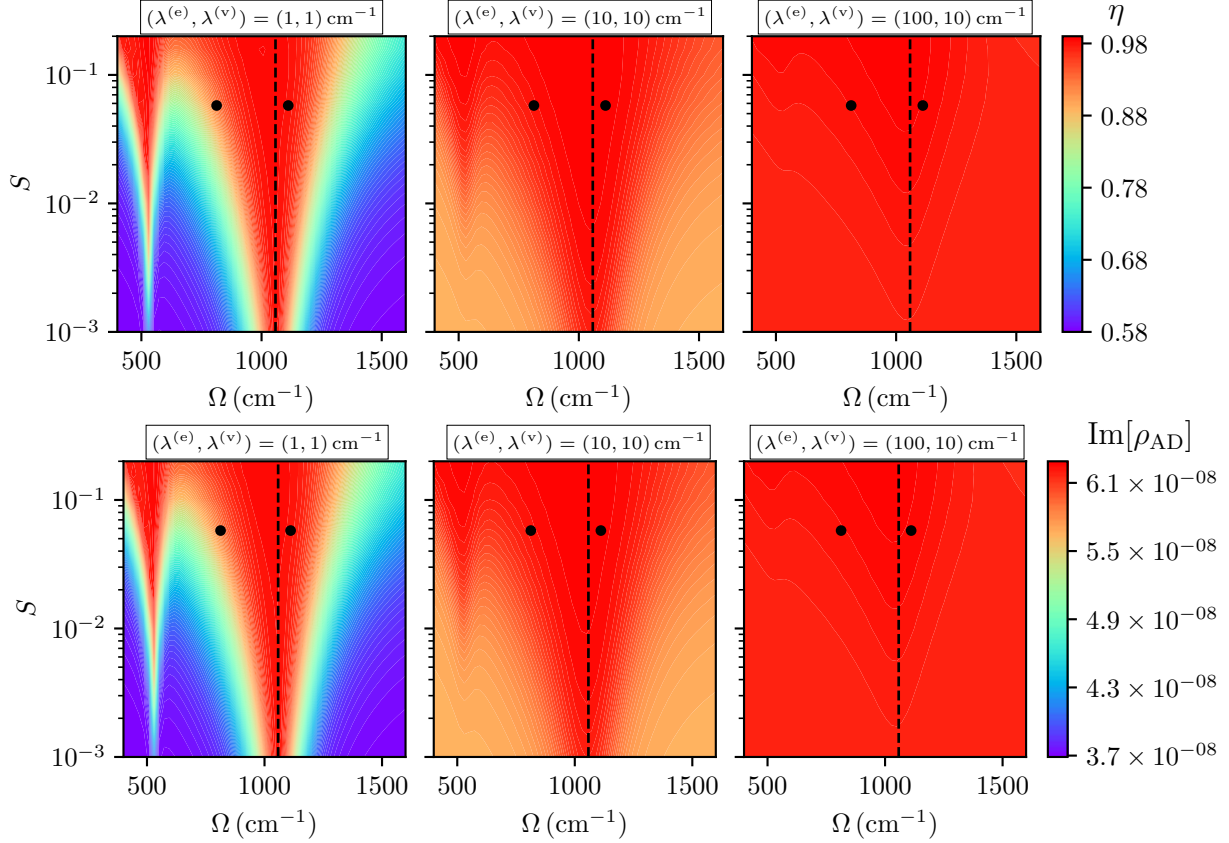


Figure 1: Quantum yield (top panels) and the imaginary part of the intersite coherence (bottom panels) as a function of the Huang-Rhys factor  $S$  and the intramolecular vibrational frequency  $\Omega$  considering different reorganization energies  $\lambda^{(e,v)}$  (system–phonon bath coupling strength). Typical values for recombination  $\tau_{\text{rec}} = 1$  ns and trapping  $\tau_{\text{trap}} = 10$  ps times are assumed.

the two black points mark the frequencies  $\Omega = 813 \text{ cm}^{-1}$  (off-resonance) and  $\Omega = 1111 \text{ cm}^{-1}$  (quasi-resonance) for the Huang-Rhys factor  $S = 0.0578$  reported in previous works.<sup>10,41</sup>

In the case of very weak coupling to the phonon baths  $(\lambda^{(e)}, \lambda^{(v)}) = (1, 1) \text{ cm}^{-1}$ , Figure 1 shows a significant change in the quantum yield and the imaginary part of the intersite coherence in the region close to the resonance frequency  $\Omega = 1058 \text{ cm}^{-1}$  and for a half of the resonance frequency  $\Omega = 529 \text{ cm}^{-1}$  for different values of the Huang-Rhys factor. The formation of a resonance pattern is observed in this case. Hence, the NESS allows for the vibronic resonance effect. However, these values for the reorganization energies are far smaller than those estimated for the real biophysical systems, which are in an intermediate coupling regime with the phonon bath, i.e.,  $\lambda^{(e)} \sim V_{AD} \sim \mathcal{G}_{A/D}$ .

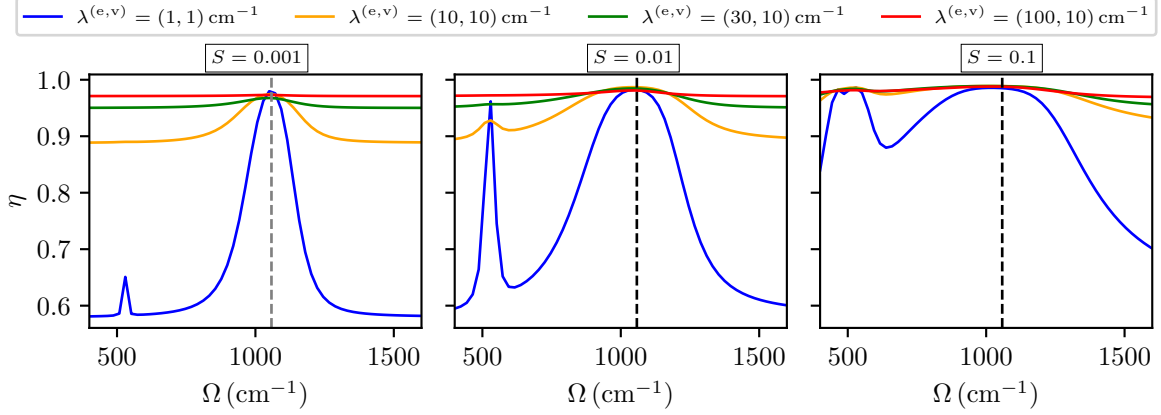


Figure 2: Quantum yield as function of the intramolecular vibrational frequency for specific values of the Huang-Rhys factor  $S = 0.001$  (left)  $S = 0.01$  (middle)  $S = 0.1$  (right) and different values of the reorganization energies  $\lambda^{(e,v)}$  (color coding is shown on the top).  $\tau_{\text{rec}} = 1$  ns and  $\tau_{\text{trap}} = 10$  ps.

As can be seen in Figure 1, as the values of system-phonon bath couplings increase, the pattern of the electronic-vibrational resonance observed for  $(\lambda^{(e)}, \lambda^{(v)}) = (1, 1) \text{ cm}^{-1}$  fades away. In fact, for realistic values of the reorganization energies, e.g.,  $(\lambda^{(e)}, \lambda^{(v)}) = (100, 10) \text{ cm}^{-1}$ , as expected for photosynthetic complexes such as the protein-antenna phycoerythrin 545, the changes in the quantum yield due to the vibronic resonance are insignificant (see also Figure 3). Therefore, in the case of realistic coupling strengths to the phonon environment in the NESS the vibronic resonance effects disappear. Comparing the upper and the bottom panels in Figure 1 it can be concluded that the changes in the quantum yield have the same trend as the imaginary part of the intersite coherence, as pointed out above in the analysis of energy transport. In other words, the current from the donor chromophore is proportional to the imaginary part of the intersite coherence  $F_{DA} = 2V_{AD} \text{Im}[\rho_{DA}]$ .

This physical picture is corroborated in Figure 2, which displays the quantum yield  $\eta$  as a function of intramolecular vibrational frequency  $\Omega$  for the Huang-Rhys factors  $S = \{0.001, 0.01, 0.1\}$  and different values of the reorganization energies (color coded). For all the Huang-Rhys factors analyzed, vibronic resonance signatures (peaks) lead to significant changes in the quantum yield only for weak system-phonon bath couplings. For the expected physical scenario where  $(\lambda^{(e)}, \lambda^{(v)}) = (100, 10) \text{ cm}^{-1}$  (red lines), there is no effect on the

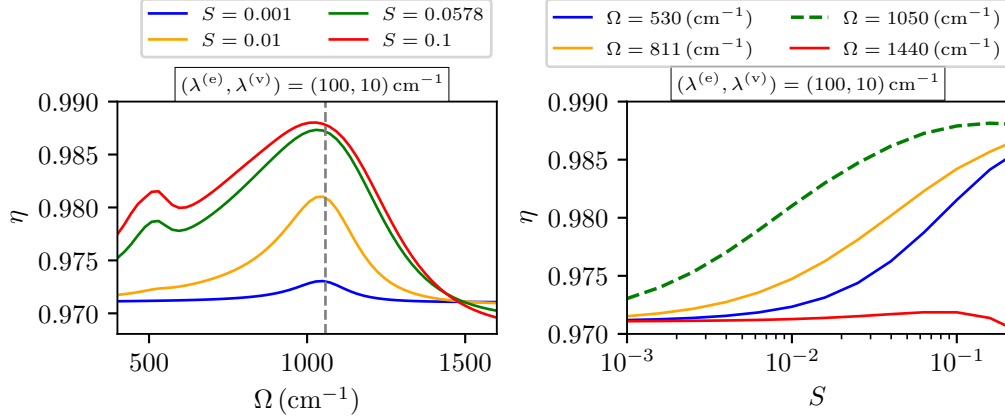


Figure 3: Quantum yield as a function of the intramolecular vibrational frequency  $\Omega$  (left) and the Huang-Rhys factor  $S$  (right) for the case  $\lambda^{(e)} = 100 \text{ cm}^{-1}$  and  $\lambda^{(v)} = 10 \text{ cm}^{-1}$  (see the top right panel in Fig. 1). Color coding is shown on the top of each figure.  $\tau_{\text{rec}} = 1 \text{ ns}$  and  $\tau_{\text{trap}} = 10 \text{ ps}$ .

quantum yield, neither with frequency changes nor changes in the Huang-Rhys factor.

Figure 3 shows detailed information on the quantum yield as a function of the intramolecular vibrational frequency (left panel) and the Huang-Rhys factor (right panel) for the case  $(\lambda^{(e)}, \lambda^{(v)}) = (100, 10) \text{ cm}^{-1}$  (corresponding to the top right panel in Fig. 1 and red lines in Fig. 2). Even though small spikes appear close to the resonance region, the changes in the quantum yield are marginal for changes in the intramolecular vibrational frequency or the Huang-Rhys factor (note the vertical scale). Analogous results are obtained for different recombination and trapping times where quantum yields are far less than one. *Therefore, when all non-unitary contributions in Eq. 5 are considered, i.e., radiation and phonon baths, exciton recombination and trapping at the reaction center, and the physical parameters are within the regime expected for the natural function, there is no significant changes in the quantum yield resulting from vibronic resonance in the NESS* (We present additional NESS results supporting the above by using the hierarchical equations of motion (HEOM) method in Figure S2 of the Supporting Information).

***Non-unitary contributions in the establishment of the NESS.***—Below we examine individual terms (recombination, trapping and phonon bath coupling) in an effort to identify the particular feature (or features) that allow the electronic-vibrational resonance

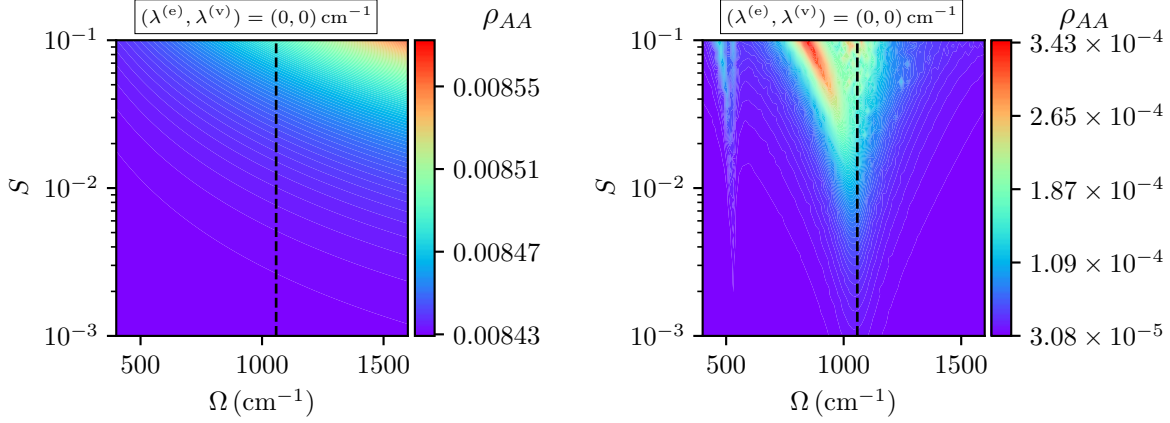


Figure 4: NESS population of the acceptor chromophore as a function of the intramolecular vibrational frequency  $\Omega$  and the Huang-Rhys factor  $S$  when the coupling strengths to the phonon baths are zero ( $\lambda^{(e)} = 0$  and  $\lambda^{(v)} = 0$ ), and there is no trapping at the reaction center. Left panel:  $\tau_{\text{rec}} = \infty$  (Incoherent light only). Right panel  $\tau_{\text{rec}} = 1$  ns (Incoherent light + recombination only).

effect. Although the natural scenario corresponds to the situation discussed above, where the exciton population is harvested at the reaction center, to quantify a possible effect due to the vibronic resonance in the case of no trapping at the reaction center, we consider the population in the acceptor chromophore  $\rho_{AA}$ .

First, consider the case where the system only interacts with the incoherent light and reaches a canonical thermal equilibrium at long times  $\hat{\rho}^{(\text{eq, RB})} = e^{-\beta^{\text{RB}} \hat{H}_{\text{sys}}} / \text{Tr} e^{-\beta^{\text{RB}} \hat{H}_{\text{sys}}}$ , where  $\beta^{\text{RB}} = 1/(k_B T^{\text{RB}})$ . Due to the high temperature of the blackbody radiation bath  $T^{\text{RB}} = 5600$  K, higher energy eigenstates get a larger population (e.g., compared with the case when the phonon baths are turned on ( $T^{\text{PB}} = 300$  K)). Thus, as expected for the vibronic dimer examined here, Figure 4 (left panel) shows that the population of the acceptor chromophore increases for higher intramolecular vibrational frequencies and Huang-Rhys factors. However, the population of the acceptor chromophore does not peak when the frequency of the intramolecular vibrational mode is in resonance with the exciton energy gap, as seen in the left panel of Figure 4. That is, the distinctive resonance pattern observed in Figure 1 for the case of very low reorganization energies is nonexistent when the system thermalizes with the incoherent photon bath only or, more generally, any singular thermal

bath. Hence, the equilibrium state reached under the effect of the incoherent radiation bath is not sensitive to the vibronic resonance effect.

However, if the system interacts with the incoherent light and is also subjected to recombination, the corresponding NESS allows for the vibronic resonance effect by facilitating the transport to the ground vibrational level in the electronically excited state of the acceptor chromophore, as seen in the right panel of Figure 4. That is, the population of the ground vibrational level in the electronically excited state of the acceptor increases in the resonance, leading to a deviation from the thermal population  $\hat{\rho}^{(\text{eq, RB})}$ . Meanwhile, the acceptor population increases when the energy frequency of the intramolecular vibrational mode is in resonance with the exciton energy gap, indicating that there is a vibronic resonance effect. Furthermore, the population in the acceptor chromophore is larger with increasing Huang-Rhys factor. On the other hand, for very low Huang-Rhys factors ( $S \leq 0.001$ ), the vibronic resonance effect is barely noticeable since the vibronic couplings are too small. Similar observations can be made if the system interacts with the incoherent light and is subjected to recombination and trapping (see Figure S3 in the Supporting Information). Formally, when  $\tau_{\text{rec}} \rightarrow \infty$  and  $\tau_{\text{trap}} \rightarrow \infty$ , then  $\mathcal{J}_{\text{rec}} \rightarrow 0$  and  $\mathcal{J}_{\text{trap}} \rightarrow 0$ ; the NESS corresponds to an equilibrium thermal state  $\rho_{\text{SS}} \rightarrow \rho^{(\text{eq, RB})}$ , and therefore  $\text{Im}[\rho_{AD}] \rightarrow 0$ . Therefore, *when the reached NESS is close to an equilibrium state, the signature pattern of the electronic-vibrational resonance does not arise.*

When the effects of incoherent light, recombination, and phonon baths are considered, there is no change in the acceptor NESS population associated with the electronic-vibrational resonance interaction. Specifically, *it is the coupling to the phonon baths that suppresses vibronic resonance effects for realistic reorganization energies* (e.g.,  $(\lambda^{(\text{e})}, \lambda^{(\text{v})}) = (100, 10) \text{ cm}^{-1}$ ). In particular, the interaction with the phonon baths is stronger than the interaction with incoherent light,<sup>34,50</sup> so that the resonance-induced effects observed in the case of ‘incoherent light + recombination only’ owing to the vibronic coupling are overshadowed by the dissipative effect of the intermolecular vibrational degrees of freedom associated

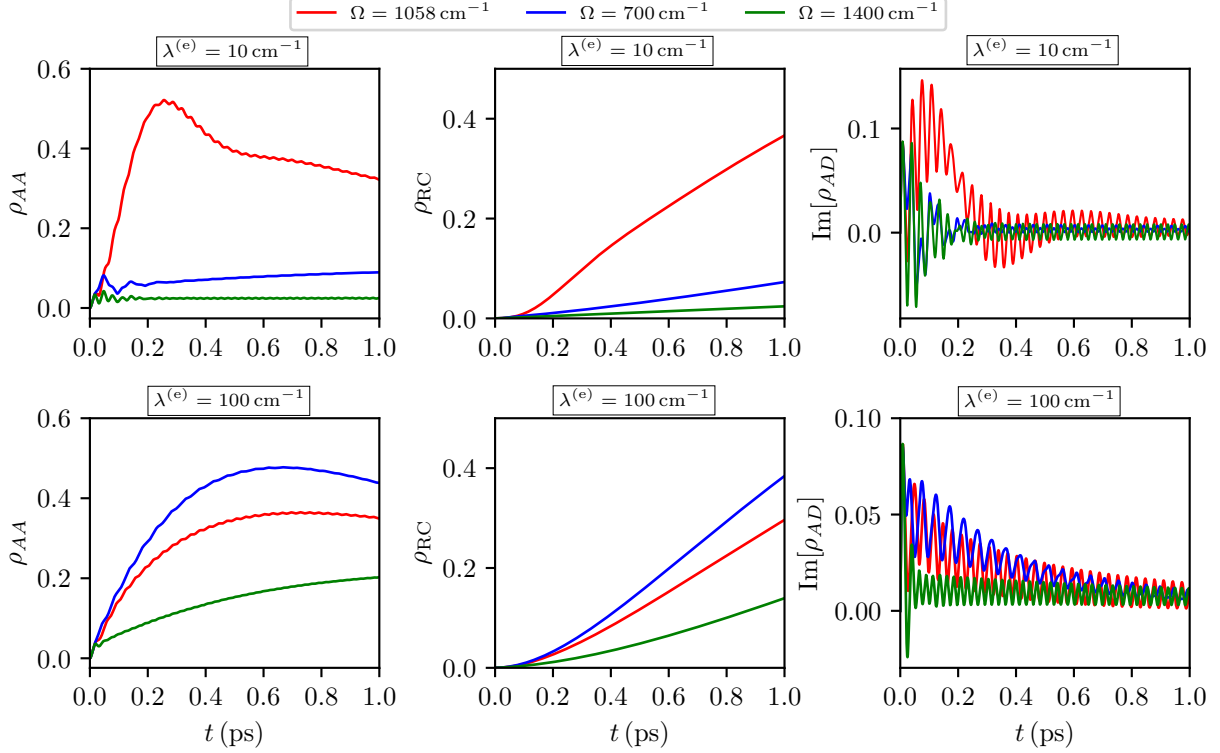


Figure 5: Population of the acceptor chromophore, population of the reaction center, and the imaginary part of the intersite coherence as a function of time for different values of the intramolecular vibrational frequency  $\Omega$  (note the color coding). Two scenarios for the system-phonon bath coupling are considered: small  $\lambda^{(e)} = 10 \text{ cm}^{-1}$  (top panels) and intermediate  $\lambda^{(e)} = 100 \text{ cm}^{-1}$  (bottom panels). For all cases, the vibronic coupling is the same  $\mathcal{G} = 250 \text{ cm}^{-1}$ .  $\tau_{\text{rec}} = 1 \text{ ns}$  and  $\tau_{\text{trap}} = 1 \text{ ps}$ .

with the low-frequency phonon baths.

**Time-dependent results: Coherent initial excitation.**— To assess the similarities regarding the vibronic resonance between NESS results discussed above and time-dependent results related to coherent light excitation discussed in the literature, Figure 5 shows the population (acceptor and reaction center) and intersite coherence (imaginary part) dynamics for times up to one picosecond, assuming an initial coherent excitation condition  $\rho_D(t=0) = 1$ , i.e., the entire population initially in the donor. The top and bottom panels in Figure 5 display the dynamics using the HEOM method (see Supporting Information) for weak and intermediate system-phonon bath coupling  $\lambda^{(e)} = 10 \text{ cm}^{-1}$  ( $\lambda^{(e)} = 100 \text{ cm}^{-1}$ ) for three intramolecular vibrational frequencies:  $\Omega = 1058 \text{ cm}^{-1}$  (on-resonance) and  $\Omega = \{700, 1400\} \text{ cm}^{-1}$  (off-

resonance). The same vibronic coupling  $\mathcal{G} = 250 \text{ cm}^{-1}$  is considered in all the cases, and typical values for recombination  $\tau_{\text{rec}} = 1 \text{ ns}$  and trapping  $\tau_{\text{trap}} = 1 \text{ ps}$  times are assumed.

For weak system-phonon bath coupling, the time-dependent results evidence an enhancement in the acceptor and the reaction center population, as well as in the imaginary part of the intersite coherence related to the flux between chromophores for the on-resonance vibrational frequency compared to the off-resonance frequencies (see top panels in Figure 5). However, for intermediate system-phonon bath coupling, the increase in the acceptor and the reaction center population, as well as in the imaginary part of the intersite coherence, is not guaranteed for the vibrational frequency on-resonance with the exciton energy gap (see red curves in bottom panels of Figure 5). In fact, higher values in the acceptor and the reaction center population, as well as in  $\text{Im}[\rho_{DA}]$ , are obtained for the off-resonance frequency  $\Omega = 700 \text{ cm}^{-1}$  (see blue curves in bottom panels of Figure 5). This is in contrast to prior work<sup>17</sup> which did not examine the lower off-resonance frequencies (here  $\Omega = 700 \text{ cm}^{-1}$ ) and concluded that a significant resonance effect exists.

We observe then that for weak system-phonon bath coupling the time-dependent results evidence an electronic-vibrational resonance effect, as observed in the case of the NESS results discussed above. For realistic values of the reorganization energy, that is, in the intermediate system-phonon bath coupling regime, the results differ from the NESS case, in that time-dependent results could lead to significantly different population and coherence dynamics as a function of the intramolecular vibrational frequency. However, it is possible to obtain higher values for the acceptor and the reaction center population for off-resonance vibrational frequencies as compared to the on-resonance vibrational frequency. These observations merit further study, ongoing in our laboratory.

**Conclusions.**—Natural incoherent light-induced processes in photosynthetic light-harvesting systems occur in a non-equilibrium steady-state (NESS). Here, the extent to which electronic-vibrational resonance associated with high-energy intramolecular vibrations affects the steady-state energy transport in the PEB dimer was analyzed using a prototype

vibronic dimer, i.e., two two-level systems, each coupled to an intramolecular vibrational mode. *The results indicate that in the NESS for the PEB dimer, intramolecular vibrations with frequency resonant with the energy difference between exciton states do not alter the quantum yield nor the imaginary part of intersite coherence relevant for transport compared to non-resonant vibrations.* The results clearly motivate studies of other relevant biological models.

Individual non-unitary contributions (incoherent light, recombination, trapping and phonon coupling) were analyzed to determine the physical feature that destroys the electronic-vibrational resonance effect. We conclude that in the natural scenario of incoherent light excitation and under realistic system-phonon bath couplings, the steady-state reached is dominated mainly by the effect of the phonon baths, and the impact of the vibronic resonance is not evident. Moreover, under initial coherent excitation, as prepared by pulsed lasers and commonly assumed in other studies about vibronic effects in photosynthetic light-harvesting systems, and considering an intermediate system-phonon bath coupling regime, it is possible to obtain higher values for the acceptor population and the imaginary part of the intersite coherence for off-resonance vibrational frequencies as compared to the on-resonance vibrational frequency. These PEB results imply that energy transport is not dramatically affected by electronic-vibrational resonance.

## Acknowledgement

This work was supported by the U.S. Air Force Office of Scientific Research (AFOSR) under Contract No. FA9550-20-1-0354.

## Supporting Information Available

Electronic dimer model; Quantum yield analysis considering a trapping time of one picosecond; presentation of NESS results using the HEOM method; Figure S3: quantum yield for

the case of incoherent light + recombination + trapping only.

## References

- (1) Renger, T.; May, V.; Kühn, O. Ultrafast excitation energy transfer dynamics in photosynthetic pigment-protein complexes. *Phys. Rep.* **2001**, *343*, 137–254.
- (2) Jonas, D. M. Two-Dimensional Femtosecond Spectroscopy. *Annu. Rev. Phys. Chem.* **2003**, *54*, 425–463.
- (3) Brixner, T.; Stenger, J.; Vaswani, H. M.; Cho, M.; Blankenship, R. E.; Fleming, G. R. Two-dimensional spectroscopy of electronic couplings in photosynthesis. *Nature* **2005**, *434*, 625–628.
- (4) Collini, E.; Wong, C. Y.; Wilk, K. E.; Curmi, P. M. G.; Brumer, P.; Scholes, G. D. Coherently wired light-harvesting in photosynthetic marine algae at ambient temperature. *Nature* **2010**, *463*, 644–647.
- (5) Jang, S. J.; Mennucci, B. Delocalized excitons in natural light-harvesting complexes. *Rev. Mod. Phys.* **2018**, *90*, 035003.
- (6) Mančal, T. A decade with quantum coherence: How our past became classical and the future turned quantum. *Chemical Physics* **2020**, *532*, 110663.
- (7) Womick, J. M.; Moran, A. M. Vibronic enhancement of exciton sizes and energy transport in photosynthetic complexes. *J. Phys. Chem. B* **2011**, *115*, 1347–1356.
- (8) Butkus, V.; Valkunas, L.; Abramavicius, D. Molecular vibrations-induced quantum beats in two-dimensional electronic spectroscopy. *J. Chem. Phys.* **2012**, *137*, 044513.
- (9) Christensson, N.; Kauffmann, H. F.; Pullerits, T.; Mančal, T. Origin of Long-Lived Coherences in Light-Harvesting Complexes. *J. Phys. Chem. B* **2012**, *116*, 7449–7454.

- (10) Kolli, A.; O'Reilly, E. J.; Scholes, G. D.; Olaya-Castro, A. The fundamental role of quantized vibrations in coherent light harvesting by cryptophyte algae. *J. Chem. Phys.* **2012**, *137*, 174109.
- (11) Chenu, A.; Christensson, N.; Kauffmann, H. F.; Mančal, T. Enhancement of vibronic and ground-state vibrational coherences in 2D spectra of photosynthetic complexes. *Sci. Rep.* **2013**, *3*, 2029.
- (12) Tiwari, V.; Peters, W. K.; Jonas, D. M. Electronic resonance with anticorrelated pigment vibrations drives photosynthetic energy transfer outside the adiabatic framework. *Proc. Natl. Acad. Sci. USA* **2013**, *110*, 1203–1208.
- (13) Chin, A. W.; Prior, J.; Rosenbach, R.; Caycedo-Soler, F.; Huelga, S. F.; Plenio, M. B. The role of non-equilibrium vibrational structures in electronic coherence and recoherence in pigment-protein complexes. *Nat. Phys.* **2013**, *9*, 113–118.
- (14) Fuller, F. D.; Pan, J.; Gelzinis, A.; Butkus, V.; Senlik, S. S.; Wilcox, D. E.; Yocum, C. F.; Valkunas, L.; Abramavicius, D.; Ogilvie, J. P. Vibronic coherence in oxygenic photosynthesis. *Nat. Chem.* **2014**, *6*, 706–711.
- (15) Butkus, V.; Valkunas, L.; Abramavicius, D. Vibronic phenomena and exciton-vibrational interference in two-dimensional spectra of molecular aggregates. *J. Chem. Phys.* **2014**, *140*, 034306.
- (16) Halpin, A.; Johnson, P. J.; Tempelaar, R.; Murphy, R. S.; Knoester, J.; Jansen, T. L.; Miller, R. D. Two-dimensional spectroscopy of a molecular dimer unveils the effects of vibronic coupling on exciton coherences. *Nat. Chem.* **2014**, *6*, 196–201.
- (17) O'Reilly, E. J.; Olaya-Castro, A. Non-classicality of the molecular vibrations assisting exciton energy transfer at room temperature. *Nat. Commun.* **2014**, *5*, 3012.

- (18) Romero, E.; Augulis, R.; Novoderezhkin, V. I.; Ferretti, M.; Thieme, J.; Zigmantas, D.; Van Grondelle, R. Quantum coherence in photosynthesis for efficient solar energy conversion. *Nat. Phys.* **2014**, *10*, 676.
- (19) Dijkstra, A. G.; Wang, C.; Cao, J.; Fleming, G. R. Coherent Exciton Dynamics in the Presence of Underdamped Vibrations. *J. Phys. Chem. Lett.* **2015**, *6*, 627–632.
- (20) Novelli, F.; Nazir, A.; Richards, G. H.; Roozbeh, A.; Wilk, K. E.; Curmi, P. M.; Davis, J. A. Vibronic resonances facilitate excited-state coherence in light-harvesting proteins at room temperature. *J. Phys. Chem. Lett.* **2015**, *6*, 4573–4580.
- (21) Schröter, M.; Ivanov, S.; Schulze, J.; Polyutov, S.; Yan, Y.; Pullerits, T.; Kühn, O. Exciton–vibrational coupling in the dynamics and spectroscopy of Frenkel excitons in molecular aggregates. *Phys. Rep.* **2015**, *567*, 1–78.
- (22) Malý, P.; Somsen, O. J.; Novoderezhkin, V. I.; Mančal, T.; Van Grondelle, R. The Role of Resonant Vibrations in Electronic Energy Transfer. *ChemPhysChem* **2016**, *17*, 1356–1368.
- (23) Dean, J. C.; Mirkovic, T.; Toa, Z. S.; Oblinsky, D. G.; Scholes, G. D. Vibronic enhancement of algae light harvesting. *Chem* **2016**, *1*, 858–872.
- (24) Yeh, S.-H.; Hoehn, R. D.; Allodi, M. A.; Engel, G. S.; Kais, S. Elucidation of near-resonance vibronic coherence lifetimes by nonadiabatic electronic-vibrational state character mixing. *Proc. Natl. Acad. Sci. U.S.A.* **2019**, *116*, 18263–18268.
- (25) Cao, J.; Cogdell, R. J.; Coker, D. F.; Duan, H.-G.; Hauer, J.; Kleinekathöfer, U.; Jansen, T. L.; Mančal, T.; Miller, R. D.; Ogilvie, J. P. et al. Quantum biology revisited. *Sci. Adv.* **2020**, *6*, eaaz4888.
- (26) Arsenault, E. A.; Yoneda, Y.; Iwai, M.; Niyogi, K. K.; Fleming, G. R. Vibronic mixing

- enables ultrafast energy flow in light-harvesting complex II. *Nat. Commun.* **2020**, *11*, 1–8.
- (27) Higgins, J. S.; Lloyd, L. T.; Sohail, S. H.; Allodi, M. A.; Otto, J. P.; Saer, R. G.; Wood, R. E.; Massey, S. C.; Ting, P.-C.; Blankenship, R. E. et al. Photosynthesis tunes quantum-mechanical mixing of electronic and vibrational states to steer exciton energy transfer. *Proc. Natl. Acad. Sci. U.S.A.* **2021**, *118*, e2018240118.
- (28) Policht, V. R.; Niedringhaus, A.; Willow, R.; Laible, P. D.; Bocian, D. F.; Kirmaier, C.; Holten, D.; Mančal, T.; Ogilvie, J. P. Hidden vibronic and excitonic structure and vibronic coherence transfer in the bacterial reaction center. *Sci. Adv.* **2022**, *8*, eabk0953.
- (29) Jiang, X.-P.; Brumer, P. Creation and dynamics of molecular states prepared with coherent vs partially coherent pulsed light. *J. Chem. Phys.* **1991**, *94*, 5833–5843.
- (30) Mančal, T.; Valkunas, L. Exciton dynamics in photosynthetic complexes: excitation by coherent and incoherent light. *New J. Phys.* **2010**, *12*, 065044.
- (31) Brumer, P.; Shapiro, M. Molecular response in one-photon absorption via natural thermal light vs. pulsed laser excitation. *Proc. Natl. Acad. Sci. U.S.A.* **2012**, *109*, 19575–19578.
- (32) Pachón, L. A.; Brumer, P. Computational methodologies and physical insights into electronic energy transfer in photosynthetic light-harvesting complexes. *Phys. Chem. Chem. Phys.* **2012**, *14*, 10094–10108.
- (33) Kassal, I.; Yuen-Zhou, J.; Rahimi-Keshari, S. Does coherence enhance transport in photosynthesis? *J. Phys. Chem. Lett.* **2013**, *4*, 362–367.
- (34) Pachón, L. A.; Botero, J. D.; Brumer, P. W. Open system perspective on incoherent excitation of light harvesting systems. *J. Phys. B* **2017**, *50*, 184003.

- (35) Brumer, P. Shedding (Incoherent) Light on Quantum Effects in Light-Induced Biological Processes. *J. Phys. Chem. Lett.* **2018**, *9*, 2946–2955.
- (36) Dodin, A.; Brumer, P. Noise-induced coherence in molecular processes. *J. Phys. B* **2021**, *54*, 223001.
- (37) Tscherbul, T. V.; Brumer, P. Non-equilibrium stationary coherences in photosynthetic energy transfer under weak-field incoherent illumination. *J. Chem. Phys.* **2018**, *148*, 124114.
- (38) Chuang, C.; Brumer, P. LH1–RC light-harvesting photocycle under realistic light–matter conditions. *J. Chem. Phys.* **2020**, *152*, 154101.
- (39) Jung, K. A.; Brumer, P. Energy transfer under natural incoherent light: Effects of asymmetry on efficiency. *J. Chem. Phys.* **2020**, *153*, 114102.
- (40) Doust, A. B.; Marai, C. N.; Harrop, S. J.; Wilk, K. E.; Curmi, P. M.; Scholes, G. D. Developing a structure–function model for the cryptophyte phycoerythrin 545 using ultrahigh resolution crystallography and ultrafast laser spectroscopy. *J. Mol. Biol.* **2004**, *344*, 135–153.
- (41) Novoderezhkin, V. I.; Doust, A. B.; Curutchet, C.; Scholes, G. D.; Van Grondelle, R. Excitation dynamics in phycoerythrin 545: modeling of steady-state spectra and transient absorption with modified Redfield theory. *Biophys. J.* **2010**, *99*, 344–352.
- (42) Blankenship, R. E. *Molecular mechanisms of photosynthesis*; WILEY, 2014.
- (43) León-Montiel, R. d. J.; Kassal, I.; Torres, J. P. Importance of excitation and trapping conditions in photosynthetic environment-assisted energy transport. *J. Phys. Chem. B* **2014**, *118*, 10588–10594.
- (44) Janković, V.; Mančal, T. Nonequilibrium steady-state picture of incoherent light-induced excitation harvesting. *J. Chem. Phys.* **2020**, *153*, 244110.

- (45) May, V.; Kühn, O. *Charge and Energy Transfer Dynamics in Molecular Systems*; John Wiley & Sons, Ltd, 2011.
- (46) Mandel, L.; Wolf, E. *Optical coherence and quantum optics*; Cambridge University Press, 1995.
- (47) Nitzan, A. *Chemical Dynamics in Condensed Phases*; Oxford University Press, 2006.
- (48) Mohseni, M.; Rebentrost, P.; Lloyd, S.; Aspuru-Guzik, A. Environment-assisted quantum walks in photosynthetic energy transfer. *J. Chem. Phys.* **2008**, *129*, 11B603.
- (49) Roden, J. J.; Whaley, K. B. Probability-current analysis of energy transport in open quantum systems. *Phys. Rev. E* **2016**, *93*, 012128.
- (50) Pachón, L. A.; Brumer, P. Incoherent excitation of thermally equilibrated open quantum systems. *Phys. Rev. A* **2013**, *87*, 022106.